Atmos. Chem. Phys., 10, 12273–12283, 2010
www.atmos-chem-phys.net/10/12273/2010/
doi:10.5194/acp-10-12273-2010

Atmospheric Chemistry and Physics

Wintertime pollution over the Eastern Indo-Gangetic Plains as observed from MOPITT, CALIPSO and tropospheric ozone residual data

J. Kar[1], M. N. Deeter[2], J. Fishman[3], Z. Liu[3,4], A. Omar[3], J. K. Creilson[1,3,*], C. R. Trepte[3], M. A. Vaughan[3], and D. M. Winker[3]

[1]Science Systems and Applications Inc., Hampton, VA, 23666, USA
[2]National Center for Atmospheric Research, Boulder, CO, USA
[3]NASA Langley Research Center, Hampton, VA, 23681, USA
[4]National Institute of Aerospace, Hampton, VA, 23666, USA
[*]currently at: American Meteorological Society, Boston, MA 02108, USA

Received: 19 August 2010 – Published in Atmos. Chem. Phys. Discuss.: 1 September 2010
Revised: 2 December 2010 – Accepted: 20 December 2010 – Published: 23 December 2010

Abstract. A large wintertime increase in pollutants has been observed over the eastern parts of the Indo Gangetic Plains. We use improved version 4 carbon monoxide (CO) retrievals from the Measurements of Pollution in the Troposphere (MOPITT) along with latest version 3 aerosol data from the Cloud-Aerosol Lidar and Infrared Pathfinder Satellite Observations (CALIPSO) lidar instrument and the tropospheric ozone residual products to characterize this pollution pool. The feature is seen primarily in the lower troposphere from about November to February with strong concomitant increases in CO and aerosol optical depth (AOD). The signature of the feature is also observed in tropospheric ozone column data. The height resolved aerosol data from CALIPSO confirm the trapping of the pollution pool at the lowest altitudes. The observations indicate that MOPITT can capture this low altitude phenomenon even in winter conditions as indicated by the averaging kernels.

1 Introduction

The Indo Gangetic Plains (IGP) straddling the north eastern parts of India near the foot hills of the Himalayas is one of the most densely populated regions on the globe, with consequent large anthropogenic emissions. In particular, the use of traditional biofuels in the rural areas along the plains leads to strong emissions of various pollutants. It is also a region with many power plants and industries, and the recent economic growth of India has led to significant increase in industrial emissions (Ghude et al., 2008). As such, the high level of pollution in this region has been the subject of several studies over the last few years using data both from ground based and space based observations as well as models (Jethva et al., 2005; Tripathi et al., 2006; Gautam et al., 2007, 2009; Beig and Ali, 2006; Roy et al., 2008; Kar et al., 2008, 2009; Clarisse et al., 2009; Kulkarni et al., 2009). Fishman et al. (2003) had found high tropospheric ozone residual (TOR) along these plains all through the year. The large sources of emission along the plains have implications also for regional pollution, as deep convection during the monsoon months can efficiently lift the pollution to the upper troposphere where it can then be transported westward along the southern edge of the Tibetan anticyclonic circulation. The latter has been observed as the Asian summer monsoon plume in satellite measurements of various trace species like CO, CH_4, ozone etc. and has been modeled as well (Kar et al., 2004; Li et al., 2005; Park et al., 2007; Lawrence et al., 2003; Lawrence and Lelieveld, 2010; Xiong et al., 2009).

In the winter months the IGP is often enveloped by thick fog and haze (Gautam et al., 2007). The prevailing winds at low altitudes (surface to ∼850 hPa) are northerly to northwesterly with low wind speeds ($<5\,ms^{-1}$) and the eastern parts of the IGP are impacted by a localized area of strong subsidence in winter (Di Girolamo et al., 2004, Jethva et al., 2005; Dey and Di Girolamo, 2010). These conditions tend to trap the pollution at low altitudes. A striking observation from the Multi-angle Imaging SpectroRadiometer (MISR) instrument aboard Terra was the high AOD in the winter

Correspondence to: J. Kar
(jayanta.kar@nasa.gov)

months over the eastern parts of the IGP, extending over the provinces of Bihar and West Bengal in India as well as over Bangladesh. As pointed out by Di Girolamo et al. (2004), this observation has strong implications for the large population residing in this area and thus calls for further work. Kar et al. (2008) using the CO retrievals from MOPITT (version 3 data) found a corresponding pool of high CO mixing ratios at 850 hPa level in the same area in winter. However, as noted by Kar et al. (2008), in all of version 3 MOPITT data, there was a persistent wide swath of data drop out along much of the IGP which did not allow the feature to be studied fully. The reason for this data drop out was not clear at that time. A much improved version 4 of MOPITT data has now become available (Deeter et al., 2010). As mentioned by Deeter et al. (2010), the use of the original training set in the MOPITT algorithm (version 3) led to non-convergence of retrievals in regions with very large CO mixing ratios. A revised training set now leads to considerably more convergent retrievals. In fact in version 4 data the large data drop out region along the IGP is no longer visible, possibly from these added retrievals in this highly polluted region. In this paper we examine wintertime pollution over the Eastern IGP using this new MOPITT CO dataset. While the phenomenon was initially noted in the MISR aerosol optical depth data and was also seen in Moderate Resolution Imaging SpectroRadiometer (MODIS) data (Jethva et al., 2005; Gautam et al., 2007), new height resolved aerosol data from CALIPSO have now become available, and these can provide further insight into the vertical distribution of the feature. We therefore use the aerosol data from the CALIPSO lidar instrument. Lastly, we utilize the tropospheric ozone columns from the TOR and tropospheric column ozone (TCO, Ziemke et al., 2006) databases to further characterize this winter time phenomenon over the eastern parts of the IGP.

2 Data

MOPITT (Drummond, 1992; Drummond et al., 2010) has been providing global measurements of CO profiles since March 2000 from NASA's Terra satellite using gas correlation radiometry and the data have been used widely to study the global distribution of CO and various transport phenomena in the troposphere. Recently a new version of the data (version 4) has been released (Deeter et al., 2010), which yield improved retrievals resulting from a more realistic a priori, essential for the optimal estimation technique employed for the CO retrieval algorithm. Specifically, a monthly mean climatology obtained from the Model for Ozone and Related chemical Tracers, version 4 (MOZART-4) chemical transport model interpolated to the location and day of the MOPITT retrievals is used in version 4 rather than the uniform a priori profile employed in version 3 (for details see Deeter et al., 2010). An additional change is that the state vector is represented in the form of log[volume mixing ratio (vmr)] rather than vmr as was done in version 3. Furthermore, the training set for the radiative transfer code was expanded by adding a set of highly-polluted profiles obtained by scaling each of the original CO profiles by a factor of two. The latter leads to valid retrievals over the locations with high CO sources, where the version 3 algorithm resulted in significant data drop outs (Deeter et al., 2010). We use the level 3 gridded monthly mean profiles (at 9 uniform pressure levels from 900 hPa to 100 hPa) from the version 4 MOPITT data. We also use aerosol products retrieved by the CALIPSO lidar instrument which has been providing height resolved aerosol information globally since 2006 (Winker et al., 2009, 2010). CALIPSO provides total attenuated backscatter profiles at 532 nm and 1064 nm and the perpendicular polarization component for 532 nm. A new version (V.3.01) of CALIPSO data has recently been released with significant improvements in the cloud-aerosol screening module as well as extended profiles below layers with strong attenuation. The new version also provides the column integrated optical depth information for the first time. The depolarization ratio from the 532 nm channel provides useful information about the shape of the aerosol particles, while the backscatter color ratio provides information on the size of the aerosol particles (Liu et al., 2008). For this study, we use the 5-km aerosol layer products. Furthermore, we use the two different sets of tropospheric column ozone data. In the empirically corrected tropospheric ozone residuals (TOR), the stratospheric column ozone (SCO) is determined by applying an empirical correction to the solar backscattered ultraviolet (SBUV) measurements (Wozniak et al., 2005) and then subtracting the resulting SCO from the total column measurements measured from the Total Ozone Mapping Spectrometer (TOMS; Fishman and Balok, 1999). Monthly mean fields of TOR are available and encompass the time period from 1979–2005 with missing data for the years 1994–1996. We also use the TCO database derived by Ziemke et al. (2006) from the ozone monitoring instrument (OMI) and the microwave limb sounder (MLS) instruments after cross calibrating the MLS SCO with OMI SCO obtained by the convective cloud differential method. These data have similar spatial resolution as the TOR data (1°x1.25°) and are available from October 2004 onwards as monthly means. We have also used AOD data from the AERONET station at Kanpur. Only the quality assured level 2 version 2 data were used for the years 2006-2009. We have also used the pressure tendency (omega) data from the National Centers for Environmental Prediction (NCEP) reanalyses (Kalnay et al., 1996).

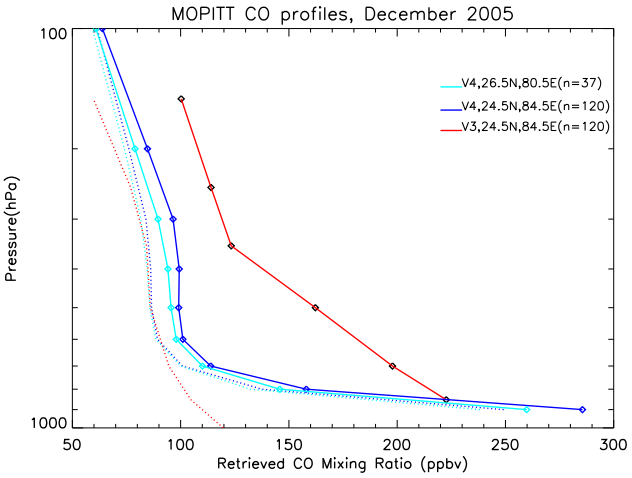

Fig. 1. MOPITT CO profiles at two locations over the Indo-Gangetic Plains (level 3 monthly mean gridded data). Note that there were no corresponding profiles within the grid cell centered at 26.5° N, 80.5° E in version 3 of MOPITT data. The dashed curves are the corresponding a priori profiles used in the CO retrievals. The number of profiles for each grid cell is shown in brackets.

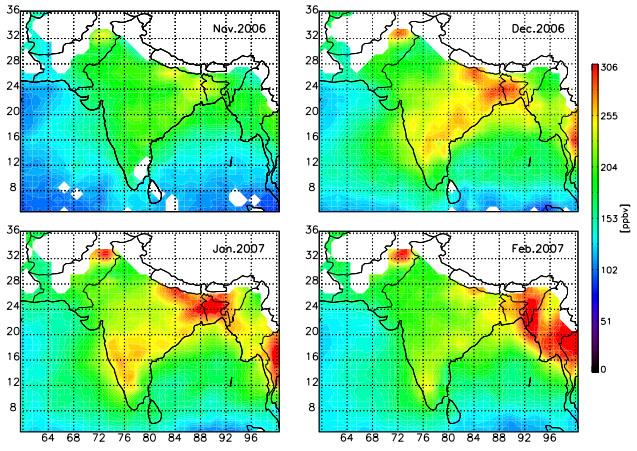

Fig. 2. Evolution of the pollution over Eastern IGP in MOPITT CO retrievals (version 4, level 3) at 900 hPa level. Only the dayside data with mean uncertainty less than 50% have been used for these plots.

3 Results

3.1 Wintertime pollution over Eastern IGP in MOPITT CO (version 4) data

Figure 1 shows a comparison of monthly mean profiles for December 2005 within the IGP area from version 3 (V3) and version 4 (V4) MOPITT data for 2 grid cells centered at 24.5° N, 84.5° E and 26.5° N, 80.5° E. Also shown are the corresponding a priori profiles from the two versions of the data (as dashed lines). The constant a priori profile in V3 differs significantly from the V4 a priori profiles below 500 hPa. The V4 mean profile at 26.5° N, 80.5° E was computed from 37 CO retrievals which were not available in V3 data and thus did not have a corresponding mean V3 profile for this grid cell. The large value of ∼260 ppbv at 900 hPa indicates that these valid retrievals in V4 may have come about because of the revised training set as mentioned above, since the cloud clearing algorithm is the same in both the versions (Deeter et al., 2010). The V4 mean profile at 24.5° N, 84.5° E, on the other hand, had a corresponding monthly mean V3 profile with the same number of profiles (120) in both the versions. The number of profiles retrieved near 26.5° N, 80.5° E is significantly less than near 24.5° N, 84.5° E, which might be attributed to higher cloud fraction near the former location as seen in the Terra MODIS data (not shown). Significant differences can be seen in the middle and lower tropospheric mixing ratios, once again with much higher values in the lowest levels in version 4. The added retrievals over the IGP area now make it possible to clearly delineate the pollution pool over the Eastern IGP during the winter months. This is shown in Fig. 2 in the spatial distribution of CO at 900 hPa between the months of November 2006 to February 2007. We have used the dayside data (with mean uncertainty less than 50%) only, as these have typically higher vertical resolution than the nightside data (Deeter et al., 2010). As can be seen, very high values of CO mixing ratios at 900 hPa develop over a large area in the north eastern parts of the IGB reaching ∼300 ppbv in December and January (∼20° N–27° N, 80° E–90° E). These enhanced CO levels are generated by various anthropogenic activities including industrial activity, vehicular emissions as well as biofuel and biomass burning. The high CO values seen over South East Asia (eastward of ∼90° E) in February are likely due to the seasonal biomass burning as evidenced by the large number of hotspots in the Along Track Scanning Radiometer (ATSR) maps over this area (not shown). Similar evolution of the feature in CO distributions at 900 hPa was also seen for other years, implying that this is a robust wintertime feature that was first seen in the MISR aerosol optical depth data (Di Girolamo et al., 2004) and was also detected in the partially available CO version 3 data from MOPITT over the region in December for various years (Kar et al., 2008). The fact that this feature was detected in the MOPITT version 3 data (at 850 hPa) as well (Kar et al., 2008), which employed a single constant a priori profile, also implies that this is indeed a robust result and cannot be simply attributed to the variable a priori employed in the version 4 data, although the a priori distributions at 900 hPa have similarities with the retrieved CO at 900 hPa (not shown).

The detection of the strong pollution over the Eastern IGP in MOPITT CO data has to be consistent with the sensitivity of MOPITT retrievals. Figure 3a (top panel) shows the monthly mean averaging kernels from MOPITT V4 data at 24.5° N, 84.5° E for all the 10 levels including the surface

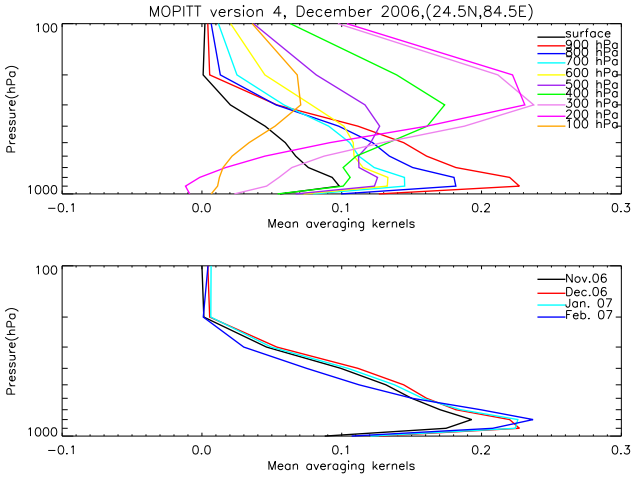

Fig. 3. (a) (top) Monthly mean averaging kernels from version 4 MOPITT data at 24.5° N, 84.5° E for December 2006 and **(b)** (bottom) Monthly mean averaging kernels at 900 hPa for November 2006 through February 2007 at the same location.

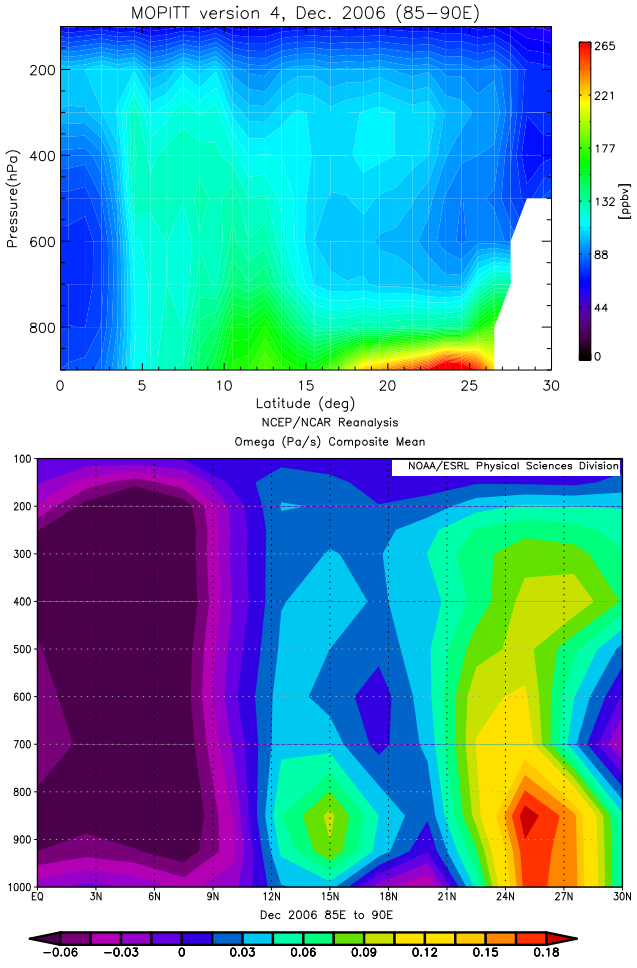

Fig. 4. (a) (top) Pressure-Latitude cross section of CO mixing ratios retrieved from MOPITT version 4 along 85° E–90° E. **(b)** (bottom) Pressure-Latitude cross section of omega (Pa/s) along 85° E–90° E from NCEP reanalyses for December 2006. Image provided by the NOAA/ESRL Physical Sciences Division, Boulder Colorado from their Web site at http://www.esrl.noaa.gov/psd/.

level for the month of December 2006. The V4 averaging kernels represent the sensitivity of the MOPITT retrievals (log(vmr) value retrieved at one level) to log(vmr) perturbations in the true profile at another level. The averaging kernels provide a measure of the vertical resolution of the retrievals (Deeter et al., 2004, 2007). The V4 averaging kernels as seen in Fig. 3a indicate significant information content in the MOPITT V4 retrievals over this area even in December with about two pieces of information. As can be seen, all the lower level kernels are peaking at the 900 hPa level, thus implying significant information coming from the lowest levels of the atmosphere. In particular, the 900 hPa kernel is sharply peaking at the same level with highest value of ∼0.23. The sharp decrease in all the kernels from 900 hPa to the surface is due to an artifact of the pressure-grid employed – the thickness of the surface layer (and thus the absorber amount perturbation) is smaller compared to those of the levels higher up except the highest one at 100 hPa (for details of this effect see Deeter et al., 2007). Figure 3b shows the monthly mean 900 hPa kernels from November 2006 to February 2007. For all months, the 900 hPa kernels peak at 800–900 hPa level.

Figure 4a shows a height latitude distribution from version 4 MOPITT CO profiles averaged over (85° E–90° E) for December 2006, while Fig. 4b shows the corresponding height latitude distribution of the pressure tendency (omega=dp/dt in Pa s^{-1}) taken from the NCEP reanalyses. While oceanic convection (negative omega) can be seen between 5° N–15° N with signatures of lifted CO into the middle troposphere, strong accumulation of pollution at the lowest altitudes occurs over the Indian landmass, consistent with the strong subsidence (positive omega) seen over the eastern IGP (∼21° N–27° N). As noted by Di Girolamo et al. (2004) and Dey and Di Girolamo (2010), the combination of strong subsidence and low wind speeds (<5 m s^{-1}) inhibits venting of this pollution above the boundary layer.

A decade of MOPITT observations makes it possible to study this feature over time. Figure 5 shows a plot of the time series of the difference between the mean CO at 900 hPa level within the Eastern IGP (∼20° N–27° N, 80° E–90° E) and that for a similar latitude range over the western parts of the country (∼20° N–27° N, 65° E–80° E). The number of profiles used to compute the means in the two regions varies from month to month. The median number of profiles for the Eastern IGP was 70 with the minimum number being 3; the median was 105 for the Western India with a minimum of 33. The difference generally increases sharply during the fall through winter months and tends to decrease during the summer months, although large scale data drop outs during the monsoon months might be biasing the results somewhat.

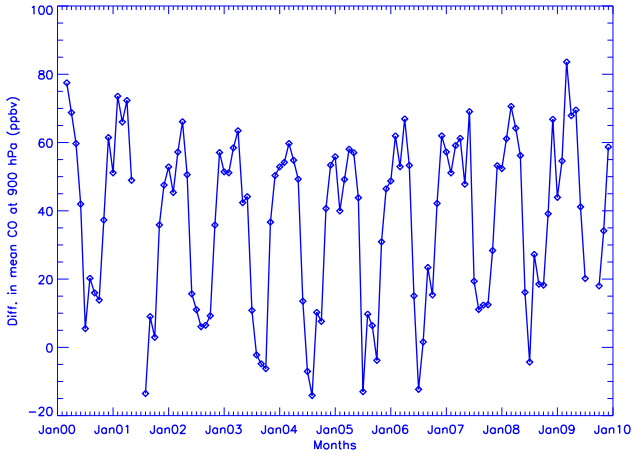

Fig. 5. Time series of the difference in mean CO at 900 hPa between the Eastern IGP (20° N–27° N, 80° E–90° E) and Western India (20° N–27° N, 65° E–80° E).

The high values often persist into March and April, possibly because of the influence of the biomass burning within India towards the eastern edge of IGP. Emissions from biomass burning in Eastern India reach a maximum in spring (Duncan et al., 2003; Streets et al., 2003).

3.2 Wintertime pollution over Eastern IGP in CALIPSO (version 3) data

Further direct evidence of the low altitude wintertime pollution comes from the CALIPSO height resolved aerosol data. Figure 6a shows the total attenuated backscatter at 532 nm on 1 January 2007 along a transect crossing the Eastern IGP area. The transect is shown in the inset in the bottom panel. Strong aerosol layers (red-grayish features) can be seen over the area from ∼20° N to the foot hills of the Himalayas, essentially confined below ∼2 km altitude range. The vertical feature mask shown in Fig. 6b indicates primarily aerosol layers over the land from 20° N to ∼28° N up to the foot hills of the Himalayas. In the Version 3 CALIPSO data, the aerosol subtypes are now directly available in the browse images. Figure 6c shows the corresponding subtype information for this scene. In the Eastern IGP, (∼20° N–28° N) several different aerosol subtypes can be discerned, with polluted continental and polluted dust at the lowest levels overlain with dust and smoke. Initial validation of the CALIPSO aerosol subtyping scheme has been conducted by Mielonen et al. (2009), who compared the CALIPSO aerosol subtyping results with corresponding aerosol types derived from the AERONET observations at 38 sites spread across the world. A good overall agreement (70%) was found between the aerosol types, with best agreement for coarse particles like dust and polluted dust and lower agreement for fine particles.

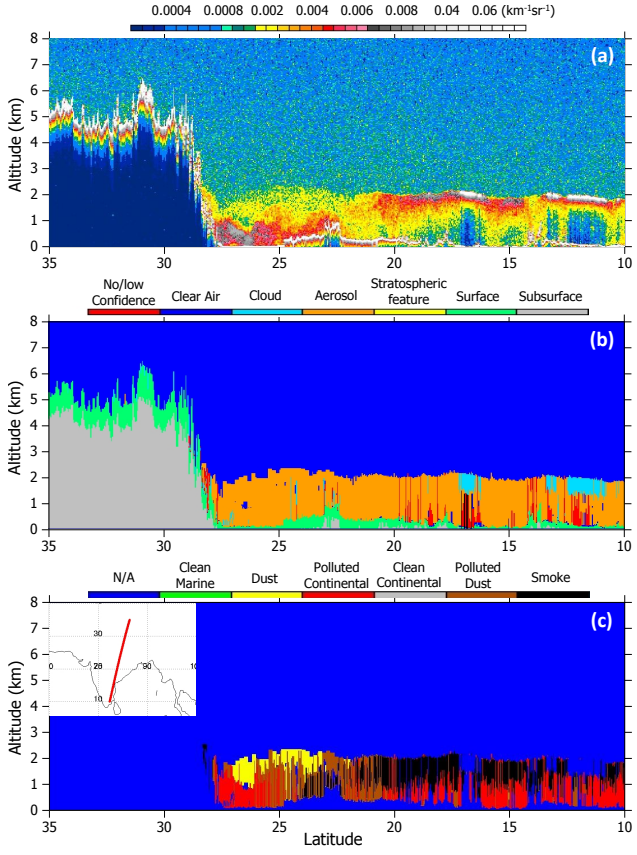

Fig. 6. a) Total attenuated backscatter at 532 nm, b) the vertical feature mask and c) the aerosol subtypes from CALIPSO (version 3.01 data) on 1 January 2007 along a transect crossing Eastern IGP showing the low altitude aerosols over this area. The transect is shown in the inset of the bottom panel.

We use the 5-km aerosol layer product from CALIPSO V3 data to characterize the aerosol environment over the Eastern IGP. Figure 7 shows the altitude distributions of the top of the layers (above surface level) in the different seasons for the year 2007. All layers between surface and 6 km with Cloud Aerosol Discrimination (CAD) score of −100 only, were included. A CAD score of −100 indicates that the layer has been identified as an aerosol layer with complete confidence (Liu et al., 2009, 2010). Significant seasonal changes in the altitude distribution can be seen. The winter (December 2006 through February 2007) distribution is clearly different from the other seasons. The maximum number of aerosol layers was detected during this season, with the bulk of them having top altitudes within 2–3 km. In contrast, a significant number of layers in spring have top altitudes in excess of 3 km. These layers are likely dust layers transported into the region from the western parts of the sub-continent. In summer the number of layers drops drastically, indicating the influence of the monsoon.

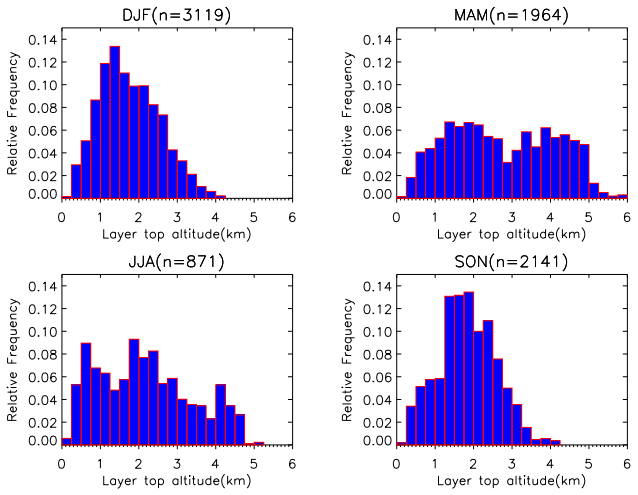

Fig. 7. Altitude of aerosol layer tops (above the surface) from CALIPSO over Eastern IGP for various seasons in 2007. The DJF plot includes data from December 2006-February 2007. Only night time data with CAD scores of −100 were used.

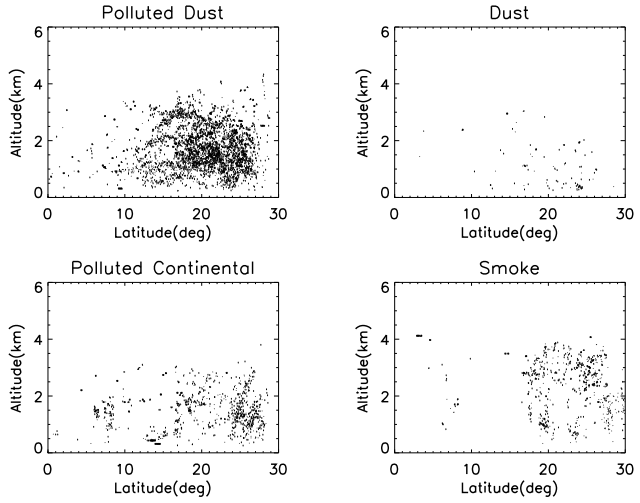

Fig. 9. Altitude distribution of the layers of dominant aerosol subtypes along 80° E-90° E between December 2006 and February 2007. Altitudes refer to top of the layers above the surface.

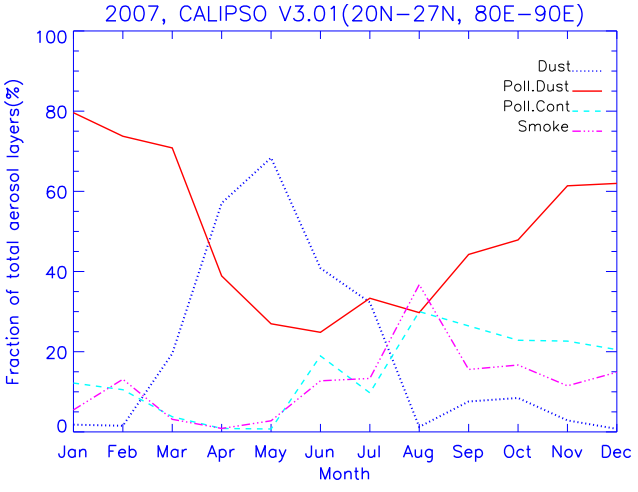

Fig. 8. Seasonal variation of the major aerosol subtypes over Eastern IGP as a fraction of the total number of aerosol layers. All night time aerosol layers with CAD scores of -100 and having layer tops less than 6 km above ground were used.

The spatial and optical properties of the aerosols, along with other ancillary data, are used to obtain the aerosol subtypes in the CALIPSO algorithm (Omar et al., 2009). Figure 8 shows the seasonal variation of the dominant subtypes (as a fraction of the total number of layers) over the Eastern IGP (∼20° N–27° N, 80° E–90° E) area during 2007. All layers with top altitudes below 6 km and CAD scores of −100 have been used for this plot. While dust dominates during spring and early summer, polluted dust seems to dominate throughout the rest of the year with smaller contributions from polluted continental and smoke. The IGP area is strongly affected by dust transported from the dry desert areas in the northwest India and Arabian peninsula during the pre-monsoon months, as has been observed from the MODIS AOD and TOMS absorbing aerosol index data, although the Eastern parts of the IGP are affected to a lesser extent (Jethva et al., 2005, Gautam et al., 2009, 2010). It should be mentioned too that the CALIPSO subtype "smoke" represents aerosols from biomass burning while polluted dust represents a mixture of "dust" and "smoke" (Omar et al., 2009). Further, the subtypes "polluted continental" and "smoke" are distinguished primarily by the requirement that "smoke" layers be elevated (i.e., as opposed to being in contact with the surface), and so occasionally there might be partial overlaps between these two groups. While dust coming from the northwestern regions declines during the monsoon months, contributions from locally generated dust (frequently mixed with 'smoke') become important during the fall and winter months. This is consistent with the findings of Dey and Di Girolamo (2010), who attribute the low Angstrom exponent and slightly higher non-spherical component of the AOD over the Eastern IGP in winter to high concentrations of coarse dust particles from rural activities. Figure 9 shows the altitudes (top of layers above the surface) of these dominant subtypes taken along a longitude belt of 80° E–90° E during the winter months (December 2006–February 2007). Once again, the low altitude aerosol layers (below 30° N) are primarily composed of polluted dust and polluted continental types, with some smoke and dust layers mixed with these.

The aerosol subtype algorithm in CALIPSO retrieval scheme primarily provides an estimate of the lidar ratio (i.e., the aerosol extinction-to-backscatter ratio) used subsequently in the extinction algorithm to obtain the layer and column integrated optical depths (Omar et al., 2009;

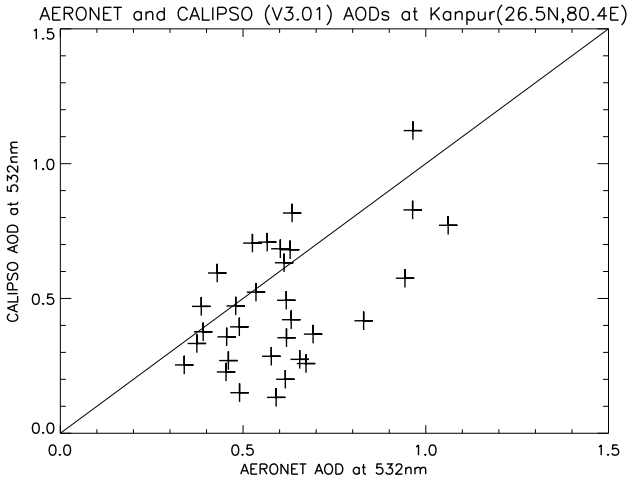

Fig. 10. Comparison of monthly mean column AODs from CALIPSO (version 3) and AERONET station at Kanpur (level 2 version 2 data). All daytime data between June 2006 and December 2009 from CALIPSO were used.

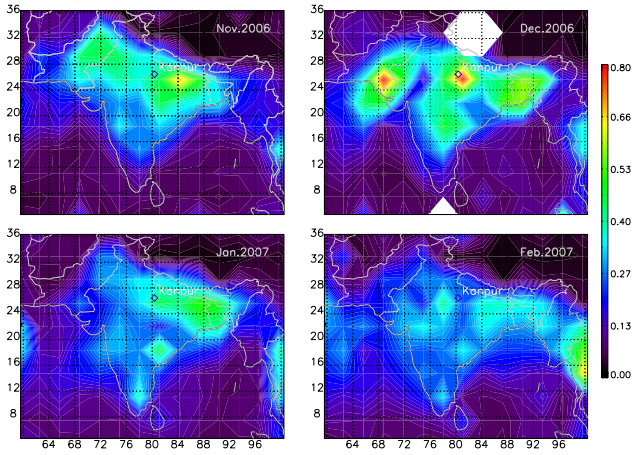

Fig. 11. Column AOD at 532 nm over Eastern IGP retrieved by CALIPSO version 3 between November 2006 and February 2007. Night time data with extinction QC value of 0 or 1 in each of the layers in the column were used.

Vaughan et al., 2010). Figure 10 shows a comparison between the monthly mean column AOD obtained from the AERONET station at Kanpur and CALIPSO. Kanpur (26.5° N, 80.4° E) is located near the northern edge of the pollution pool over Eastern IGP. Only the quality assured level 2 version 2 data from the AERONET database have been used here for the time period from June 2006 to December 2009. We used a coincidence box of $0.5° \times 0.5°$ in latitude and longitude around the location of Kanpur and used the daytime 532 nm column AOD data from CALIPSO for this comparison. The CALIPSO AOD data were filtered using two criteria: (a) the column AOD uncertainty had to be less than the column AOD value and (b) the extinction QC values for all of the layers within a particular column had to be either 0 or 1. The AERONET monthly mean data at 500 nm were interpolated to 532 nm using the Angstrom exponent in the range 440–675 nm. There were a total of 32 points available for this comparison. The comparison in Fig. 10 shows a reasonable agreement between the two data sets (linear correlation coefficient ∼0.5) with CALIPSO generally retrieving lower optical depths. It should be mentioned that we have not filtered the CALIPSO data for presence of overlying clouds because of the few data points available for comparison.

Figure 11 shows the spatial distribution of AOD at 532 nm from CALIPSO V3 over India between November 2006 and February 2007. Only night time data were used because of generally low SNR in the dayside CALIPSO data, which is caused by high levels of solar background light. Once again, the AOD data were filtered using the two criteria stated in the last paragraph. The data were binned in 3.636° in latitude and 3.06° in longitude, which ensures uniform sampling within each grid cell. Because of the sparse sampling of CALIPSO, the fine details of these plots should be viewed with some caution. However, it is clear that the spatial pattern is generally similar to the CO distribution from MOPITT, with a plume of high AOD (∼0.6) over the Eastern IGP (20° N–27° N, 80° E–90° E). The AOD values are quite similar to the maximum AOD values of about 0.6 reported over this region from the MISR instrument at 558 nm in winter as well as from MODIS at 550 nm in this area (Di Girolamo et al., 2004, Jethva et al., 2005, Dey and Di Girolamo, 2010). CALIPSO data were not available from 5–18 December 2006. The pollution plume over the Eastern IGP is well delineated in November through January and decreases in strength in February. This result attests to the fidelity of the CALIPSO AOD retrievals over this highly polluted area. Once again, we used all data for this plot without filtering for overlying clouds. However, we examined the effect of clouds by retaining only the cloud free data (cloud column optical depth = 0). While this led to data dropouts, it did not affect the overall interpretation of the results. Furthermore, the wintertime pollution pool over the Eastern IGP was seen in CALIPSO AOD data in other years as well with some inter annual variation, thus suggesting that it is a robust feature (not shown).

3.3 Wintertime pollution over Eastern IGP in the tropospheric column ozone data

The large regional enhancement of CO and aerosol at low altitudes over the Eastern IGP in winter may have implications for ozone levels in the area. We examined the tropospheric column ozone over this area using both the TOR and TCO data. Figure 12 (top panel) shows an example of regionally enhanced TOR values over the Eastern IGP in January 2006. Note the highest TOR values (∼40 DU, $1\,\text{DU} \equiv 2.69 \times 10^{16}$ molecules per cm^2) occur essentially over

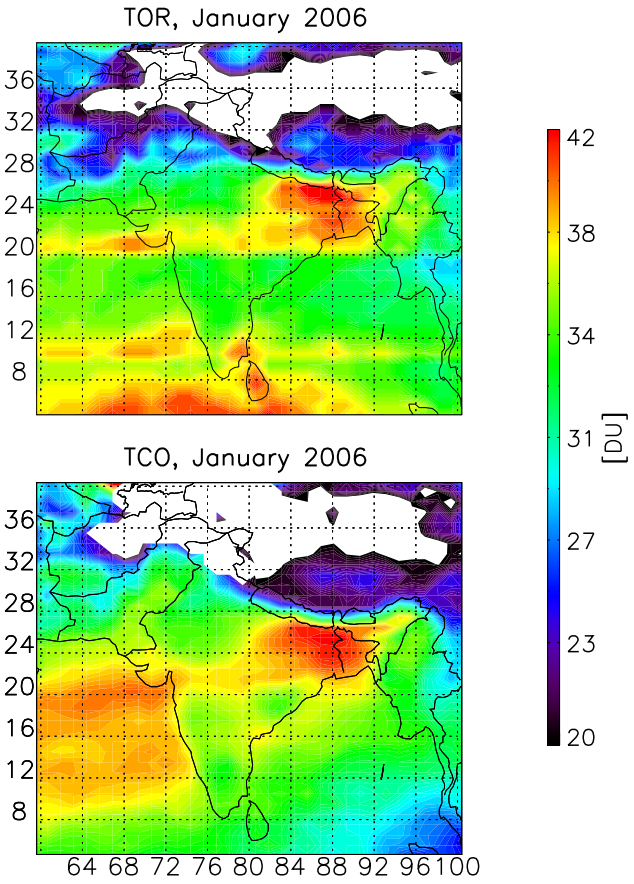

Fig. 12. Distribution of the tropospheric ozone column from TOR (top panel) and TCO (bottom panel) for January 2006.

the area where CO is regionally strongly enhanced. Figure 12 (bottom panel) shows the corresponding plume as seen in the TCO distribution. The close similarity between the spatial distributions from two different tropospheric residual products lends credence to this feature in ozone, and perhaps implies that the two products are capturing low altitude ozone produced from the enhanced levels of precursors like CO over this area at this time. The TOR values in 2006 were estimated by subtracting the SCO obtained from the Global Forecast System (GFS) model (which assimilates SBUV information) from the total ozone column retrieved by the OMI instrument. Thus the primary information on the troposphere is coming from the OMI instrument for both TOR and TCO for January 2006, and should be linked to the vertical sensitivity of the total ozone column retrievals from the OMI measurements. The latter has been quantified in terms of an "efficiency factor" and is reported in the level 2 data products of OMI at 11 levels corresponding to the midpoints of the Umkehr layers (at 2.8, 7.9, 12.5, 17.0, 21.3, 25.8, 30.4, 35.2, 40.2, 45.5, 51.0 km) and represents the sensitivity of the total ozone column to perturbations in a particular layer. The value of the efficiency factor at the lowest level (2.8 km)

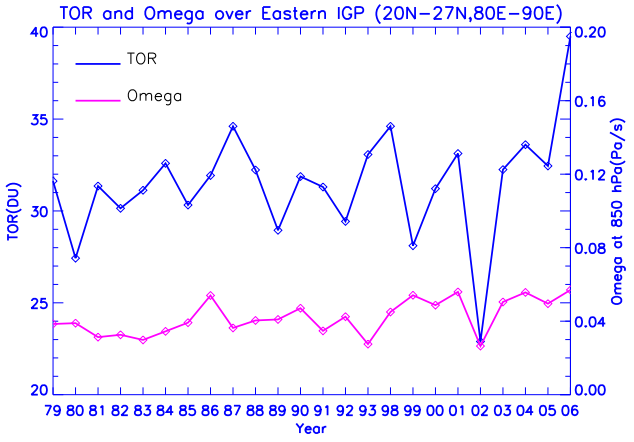

Fig. 13. TOR in January over Eastern IGP from 1979-2006 and the corresponding pressure tendency (omega, from the NCEP reanalyses). Positive values of omega indicate subsidence over the area for all years. Note that TOR data are not available from 1994 to 1997.

averaged over 20° N–27° N, 80° E–90° E for January 2006 comes out to be about 0.5, and its spatial distribution shows regionally enhanced values of the efficiency factor along the IGP (not shown). Therefore it is possible that both TOR and TCO are capturing some of the enhancements of low altitude ozone in this area in winter. Both TOR (1979-2005) and TCO (2004–2008) climatologies show enhanced ozone over Eastern IGP during the winter (December, January and February) months (not shown). While both show regional enhancements of about 3–4 DU, there are significant differences in absolute values and spatial patterns in the two maps. In TOR data, there is enhanced ozone along the entire IGP, while the TCO distribution shows more localized enhancements covering the Eastern IGP. The reason for these anomalies between TOR and TCO distributions is not clear, but may have to do with the ways the SCOs are determined in the two methods. A more thorough analysis of this is beyond the scope of this work.

Given the level of pollution in this highly populated area, it is pertinent to explore the long term tropospheric ozone over Eastern IGP. This information is available from the nearly 25 years of TOR data from 1979 to 2006 (except for the years 1994–1996). Figure 13 shows the inter-annual variation of TOR for the month of January over Eastern IGP. A modest inter-annual variation can be seen with TOR typically varying by ∼5 DU mostly. However, no significant overall trend can be discerned in the data. Also plotted in Fig. 13 are the corresponding monthly mean values of omega at the 850 hPa level. The positive omega values imply a persistent subsidence, which would promote in situ photochemical generation of tropospheric O_3 (Fishman et al., 2005). Apart from the abundance of the precursors like CO and meteorology, the TOMS efficiency factors may also determine how much of the low level O_3 is seen in the TOR in different months.

4 Conclusions

The extensive pollution along the eastern parts of the IGP during winter months has been studied using the improved version 4 CO data from MOPITT and the new version 3 height resolved aerosol data from CALIPSO as well as the tropospheric column ozone from 2 different data products. The new CO data show very high mixing ratios in the lower troposphere that primarily develop during November-February. Both the CO and aerosol data confirm the trapping of pollution at low altitudes by subsidence. Furthermore, the TOR and TCO residual ozone column data show similar spatial distributions of enhanced ozone over this area. The latter indicates that the TOR and TCO data are capturing some of the ozone being produced locally by photochemistry from the precursors at low altitudes and thus implies their usefulness for monitoring air quality in highly polluted areas. Overall these new satellite data confirm very high anthropogenic pollution over Eastern IGP in winter and call for continual monitoring and mitigation strategies.

Acknowledgements. We are grateful to Jerry Ziemke for providing the tropospheric column ozone data through the NASA Goddard tropospheric ozone website. We thank Brent Holben and R. P. Singh who had established the AERONET station at Kanpur (R.P.S was P.I till 2007) and the current P. I. S. N. Tripathi and his staff for their efforts in establishing and maintaining the Kanpur AERONET site. J. K. thanks Jean-Paul Vernier for discussions and Ralph Kuehn for a useful suggestion on binning of CALIPSO data.

Edited by: P. Monks

References

Beig, G. and Ali, K.: Behavior of boundary layer ozone and its precursors over a great alluvial plain of the world: Indo-Gangetic plains, Geophys. Res. Lett., 33, L24813, doi:10.1029/2006GL028352, 2006.

Clarisse, L., Clerbaux, C., Dentener, F., Hurtmans, D., and Coheur, P.-F.: Global ammonia observations derived from infrared satellite observations, Nature Geosci., 2, 479–483, doi:10.1038/NGEO551, 2009.

Deeter, M. N., Emmons, L. K., Edwards, D. P., Gille, J. C. and Drummond, J. R.: Vertical resolution and information content of CO profiles retrieved by MOPITT, Geophys. Res. Lett., 31, L15112, doi:10.1029/GL020235, 2004.

Deeter, M. N., Edwards, D. P., Gille, J. C., and Drummond, J. R.: Sensitivity of MOPITT observations to carbon monoxide in the lower troposphere, J. Geophys. Res., 112, D24306, doi:10.1029/2007JD008929, 2007.

Deeter, M. N., Edwards, D. P., Gille, J. C., Emmons, L. K., Francis, G., Ho, S.-P., Mao, D., Masters, D., Worden, H., Drummond, J. R., and Novelli, P. C.: The MOPITT version 4 CO product: Algorithm enhancements, validation and long-term stability, J. Geophys. Res., 115, D07036, doi:10.1029/2009JD013005, 2010.

Di Girolamo, L., Bond, T. C., Bramer, D., Diner, D. J., Fettinger, F., Kahn, R. A., Martonchik, J. V., Ramana, M. V., Ramanathan, V., and Rasch, P. J.: Analysis of multi-angle imaging spectroradiometer (MISR) aerosol optical depths over greater India during winter 2001–2004, Geophys. Res. Lett., 31, L23115, doi:10.1029/2004GL0211273, 2004.

Dey, S. and Di Girolamo, L.: A climatology of aerosol optical and microphysical properties over the Indian subcontinent from nine years (2000–2008) of Multiangle Imaging SpectroRadiometer (MISR) data, J. Geophys. Res., 115, D15204, doi:10.1029/2009JD013395, 2010.

Drummond, J. R.: Measurements of pollution in the troposphere, in The Use of EOS for studies of Atmospheric Physics, edited by: Gille, J. C. and Visconti, G., 77–101, North-Holland, Amsterdam, The Netherlands, 1992.

Drummond, J. R., Zou, J., Nichitiu, F., Kar, J., Deschambaut, R. and Hackett, J.: A review of 9-year performance and operation of the MOPITT instrument, Adv. Space Res., 45, 760–774, doi:10.1016/j.asr.2009.11.019, 2010.

Duncan, B. N., Martin, R. V., Staudt, A. C., Yevich, R. and Logan, J. A., Interannual and seasonal variability of biomass burning emissions constrained by satellite observations, J. Geophys. Res., 108(D2), 4100, doi:10.1029/2002JD002378, 2003.

Fishman, J. and Balok, A. E.: Calculation of daily tropospheric ozone residuals using TOMS and empirically improved SBUV measurements: Application to an ozone pollution episode over the eastern United States, J. Geophys. Res., 104, 30319–30340, 1999.

Fishman, J., Wozniak, A. E., and Creilson, J. K.: Global distribution of tropospheric ozone from satellite measurements using the empirically corrected tropospheric ozone residual technique; Identification of the regional aspects of air pollution, Atmos. Chem. Phys., 3, 893–907, doi:10.5194/acp-3-893-2003, 2003.

Fishman, J., Creilson, J. K., Wozniak, A. E., and Crutzen, P. J.: Interannual variability of stratospheric and tropospheric ozone determined from satellite measurements, J. Geophys. Res., 110, D20306, doi:10.1029/2005JD005868, 2005.

Gautam, R., Hsu, N. C., Kafatos, M., and Tsay, S.-C.: Influences of winter haze on fog/low cloud cover over the Indo-Gangetic plains, J. Geophys. Res., 1112, D05207, doi:10.1029/2005JD007036, 2007.

Gautam, R., Liu, Z., Singh, R. P., and Hsu, N. C. : Two contrasting dust-dominant periods over India observed from MODIS and CALIPSO data, Geophys. Res. Lett., 36, L06813, doi:10.1029/2008GL036967, 2009.

Gautam, R., Hsu, N. C., and Lau, K.-M., Premonsoon aerosol characterization and radiative effects over the Indo-Gangetic Plains: Implications for regional climate warming, J. Geophys. Res., 115, D17208, doi:10.1029/2010JD013819, 2010.

Ghude, S., Fadnavis, S., Beig, G., Polade, S. D. and van der A, R. J. : Detection of surface emission hot spots, trends, and seasonal cycle from satellite-retrived NO_2 over India, J. Geophys. Res., 113, D20305, doi:10.1029/2007JD009615., 2008.

Jethva, H., Satheesh, S. K. and Srinivasan, J.: Seasonal variability of aerosols over the Indo-Gangetic plains, J. Geophys. Res., 110, D21204, doi:10.1029/2005JD005938, 2005.

Kalnay, E., Kanamitsu, M., Kistler, R., Collins, W., Deaven, D., Gandin, L., Iredell, M., Saha, S., White, G., Woollen, J., Zhu, Y., Chelliah, M., Ebisuzaki, W., Higgins, W., Janowiak, J., Mo, K. C., Ropelewski, C., Wang, J., Leetmaa, A., Reynolds, R., Roy,J., and Joseph, D.: The NCEP/NCAR 40-Year Reanalysis Project,

B. Am. Meteorol. Soc., 77(3), 437–471, 1996.

Kar, J., Bremer, H., Drummond, J. R., Rochon, Y. J., Jones, D. B. A., Nichitiu, F., Zou, J., Liu, J., Gille, J. C., Edwards, D. P., Deeter, M. N., Francis, G., Ziskin, D., and Warner, J.: Evidence of vertical transport of carbon monoxide from measurements of pollution in the troposphere (MOPITT), Geophys. Res. Lett., 31, L23105, doi:10.1029/2004GL021128, 2004.

Kar, J., Jones, D. B. A., Drummond, J. R., Attie, J. L., Liu, J., Zou, J., Nichitiu, F., Seymour, M. D., Edwards, D. P., Deeter, M. N., Gille, J. C., and Richter, A.: Measurement of low altitude CO over the Indian subcontinent by MOPITT, J. Geophys. Res., 113, D16307, doi;10.1029/2007JD009362, 2008.

Kar, J., Jones, D. B. A., and Drummond, J. R. : Comment on "Seasonal distribution of ozone and its precursors over the tropical Indian region using regional chemistry-transport model", by Sompriti Roy et al., J. Geophys. Res., 114, D19303, doi:10.1029/2009JD011742, 2009.

Kulkarni, P. S., Jain, S. L., Ghude, S. D., Arya, B. C., Dubey, P. K., and Shahnawaz: On some aspects of tropospheric ozone variability over the Indo-Gangetic (IG) basin, India, Int. J. Remote Sens., 30(15–16), 4111–4122, 2009.

Lawrence, M. G. and Lelieveld, J.: Atmospheric pollutant outflow from southern Asia: A review, Atmos. Chem. Phys., 10, 11017–11096, doi:10.5194/acp-10-11017-2010, 2010.

Lawrence, M. G., Rasch, P. J., von Kuhlmann, R., Williams, J., Fischer, H., de Reus, M., Lelieveld, J., Crutzen, P. J., Schultz, M., Stier, P., Huntrieser, H., Heland, J., Stohl, A., Forster, C., Elbern, H., Jakobs, H., and Dickerson, R. R.: Global chemical weather forecasts for field campaign planning: Predictions and observations of large scale features during MINOS, CONTRACE and INDOEX, Atmos. Chem. Phys., 3, 267–289, 2003, http://www.atmos-chem-phys.net/3/267/2003/.

Li., Q., Jiang, J. H., Wu, D. L., Read, W. G., Livesey, N. J., Waters, J. W., Zhang, Y., Wang, B., Filipiak, M. J., Davis, C. P., Turquety, S., Wu. S., Park, R. J., Yantosca, R. M. and Jacob, D. J.: Convective outflow of south Asian pollution: A global CTM simulation compared with EOS MLS observations, Geophys. Res. Lett., 32, L14826, doi;10.1029/2005GL022762, 2005.

Liu, Z., Liu, D., Huang, J., Vaughan, M., Uno, I., Sugimoto, N., Kittaka, C., Trepte, C., Wang, Z., Hostetler, C., and Winker, D.: Airborne dust distribution over the Tibetan Plateau and surrounding areas derived from the first year of CALIPSO lidar observations, Atmos. Chem. Phys., 8, 5045–5060, doi:10.5194/acp-8-5045-2008, 2008.

Liu, Z., Vaughan, M. A., Winker, D. M., Kittaka, C., Kuehn, R. E., Getzewich, B. J., Trepte, C. R., and Hostetler, C. A.: The CALIPSO Lidar Cloud and Aerosol Discrimination: Version 2 Algorithm and Initial Assessment of Performance", J. Atmos. Ocean. Technol., 26, 1198–1213, doi:10.1175/2009JTECHA1229.1, 2009.

Liu, Z., Kuehn, R., Vaughan, M., Winker, D., Omar, A., Powell, K., Trepte, C., Hu, Y., and Hostetler, C.: The CALIPSO Cloud And Aerosol Discrimination: Version 3 Algorithm and Test Results, 25th International Laser Radar Conference (ILRC), St. Petersburg, Russia, available online at http://www-calipso.larc.nasa.gov/resources/pdfs/ILRC_LaRC_2010/Liu_ILRC25_2010.pdf), 2010.

Mielonen, T., Arola, A., Komppula, M., Kukkonen, J., Koskinen, J., de Leeuw, G., and Lehtinen, K. E. J.: Comparison of CALIOP level 2 aerosol subtypes to aerosol types derived from AERONET inversion data, Geophys. Res. Lett., 36, L18804, doi:10.1029/2009GL039609, 2009.

Omar, A. H., Winker, D. M., Kittaka, C., Vaughan, M. A., Liu, Z., Hu, Y., Trepte, C. R., Rogers, R. R., Ferrare, R. A., Lee, K-P, Kuehn, R., and Hostetler, C. A.: The CALIPSO automated aerosol classification and lidar ratio selection algorithm, J. Atmos. Ocean. Technol., 26, 1994–2014, 2009.

Park, M., Randel, W. J., Gettelman, A., Massie, S. T., and Jiang, J. H.: Transport above the Asian summer monsoon anticyclone inferred from Aura Microwave Limb Sounder tracers, J. Geophys. Res., 112, D16309, doi:10.1029/2006JD008294, 2007.

Roy, S., Beig. G., and Jacob, D.: Seasonal distribution of ozone and its precursors over the tropical Indian region using regional chemistry-transport model, J. Geophys. Res., 113, D21307, doi:10.1029/2007JD009712, 2008.

Streets, D. G., Yarber, K. F., Woo, J.-H., and Carmichael, G. R.: Biomass burning in Asia: Annual and seasonal estimates and atmospheric emissions, Global Biogeochem. Cycles, 17(4), 1099, doi:10.1029/2003GB002040, 2003.

Tripathi, S. N., Tare, V., Chinnam, N., Srivastava, A. K., Dey, S., Agarwal, A., Kishore, S., Lal, R. B., Manar, M., Kanawade, V. P., Chauhan, S. S. S., Sharma, M., Reddy, R. R., Rama Gopal, K., Narasimhulu, K., Reddy, L. S. S., Gupta, S., and Lal, S.: Measurements of atmospheric parameters during Indian Space Research Organization Geosphere Biosphere Programme Land Campaign II at a typical location in the Ganga basin: 1. Physical and optical properties, J. Geophys. Res., 111, D23209, doi:10.1029/2006JD007278, 2006.

Vaughan, M., Kuehn, R., Tackett, J., Rogers, R., Liu, Z., Omar, A., Getzewich, B., Powell, K., Hu, Y., Young, S., Avery, M., Winker, D., and Trepte, C.: Strategies for Improved CALIPSO Aerosol Optical Depth Estimates, 25th International Laser Radar Conference (ILRC), St. Petersburg, Russia. (available at http://www-calipso.larc.nasa.gov/resources/pdfs/ILRC_LaRC_2010/Vaughan_ILRC25_2010.pdf), 2010.

Winker, D. M., Vaughan, M. A., Omar, A., Hu, Y., Powell, K. A., Liu, Z., Hunt, W. H., and Young, S. A.: Overview of the CALIPSO mission and CALIOP data processing algorithms, J. Atmos. Ocean. Tech., 26, 2310–2322, 2009.

Winker, D. M., Pelon, J., Coakley Jr., J. A., Ackerman, S. A., Charlson, R. J., Colarco, P. R., Flamant, P., Fu, Q., Hoff, R. M., Kittaka, C., Kubar, T. L., Le Treut, H., McCormick, M. P., Megie, G., Poole, L., Powell, K., Trepte, C., Vaughan, M. A., and Wielicki, B. B.: The CALIPSO mission: A Global 3D view of aerosols and clouds, Bull. Amer. Meteor. Soc., 91, 1211–1229, 2010.

Wozniak, A. E., Fishman, J., Wang, P.-H., and Creilson, J. K.: The Distribution of Stratospheric Column Ozone (SCO) Determined from Satellite Observations: Validation of Solar Backscattered Ultraviolet (SBUV) Measurements in Support of the Tropospheric Ozone Residual (TOR) Method, J. Geophys. Res., 110, D20305, doi:10.1029/2005JD005868, 2005.

Xiong, X., Houweling, S., Wei, J., Maddy, E., Sun, F., and Barnet, C.: Methane plume over South Asia during the monsoon season: Satellite observation and model simulation, Atmos. Chem. Phys., 9, 783–794, doi:10.5194/acp-9-783-2009, 2009.

Ziemke, J. R., Chandra, S., Duncan, B. N., Froidevaux, L., Bhartia, P. K., Levelt, P. F., and Waters, J. W.: Tropospheric ozone

determined from Aura OMI and MLS: Evaluation of measurements and comparison with the Global Modeling Initiative's Chemical Transport Model, J. Geophys. Res., 111, D19303, doi:10.1029/2006JD007089, 2006.